UNDERSTANDING SEXTUPOLE PART III: Large Amplitude Dynamics and Dynamic Aperture

Tim Zolkin[1] Sergei Nagaitsev[2] Ivan Morozov[3]
Sergei Kladov[4] Young-Kee Kim[4]

[1]FNAL

[2]BNL, JLAB & ODU

[3]NSTU

[4]UChicago

November 12, 2024

With Deepest Respect to the Memory of Slava Danilov
(21 Jan, 1966 – 30 Dec, 2014)

Structure of presentation

1. Hénon vs. McMillan mappings
2. Perturbation theory
3. Comparing stability diagrams
4. Accelerator lattice with thin sextupole
5. Summary

Cornell University

arXiv > nlin > arXiv:2410.10380

Nonlinear Sciences > Exactly Solvable and Integrable Systems

[Submitted on 14 Oct 2024]

Dynamics of McMillan mappings III. Symmetric map with mixed nonlinearity

Tim Zolkin, Sergei Nagaitsev, Ivan Morozov, Sergei Kladov, Young-Kee Kim

1.1 Hénon map

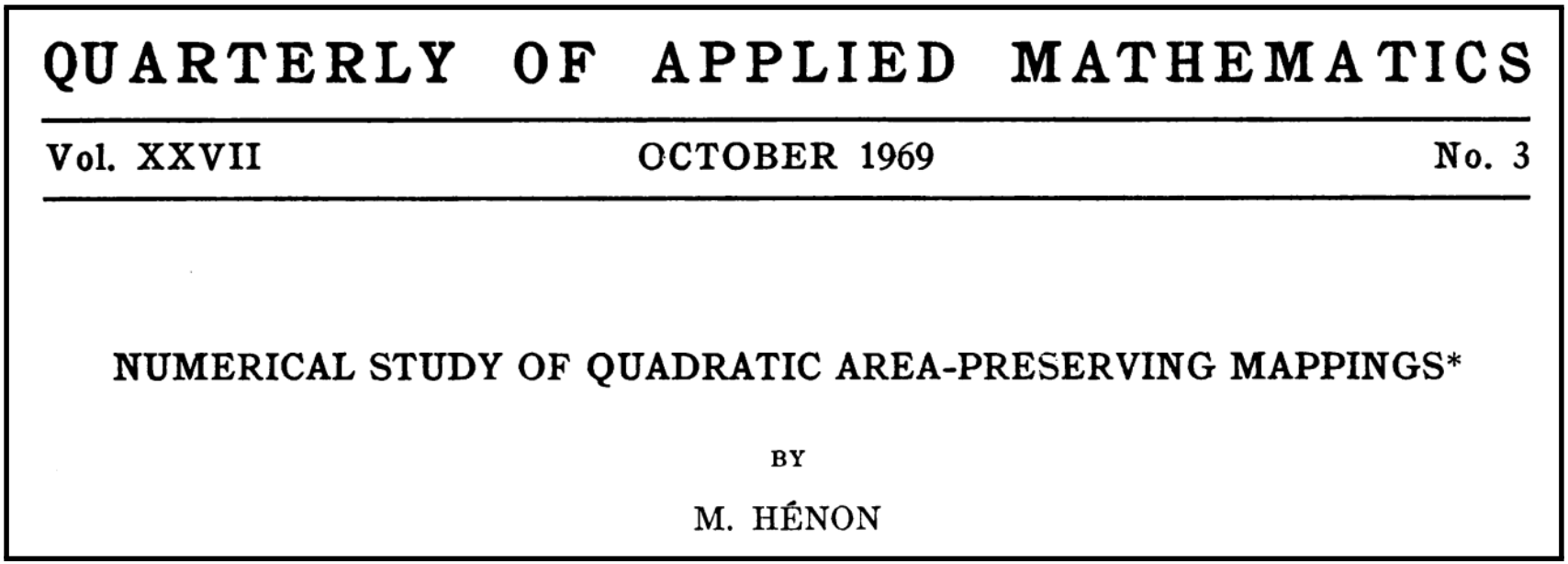

QUARTERLY OF APPLIED MATHEMATICS

Vol. XXVII OCTOBER 1969 No. 3

NUMERICAL STUDY OF QUADRATIC AREA-PRESERVING MAPPINGS*

BY

M. HÉNON

Entire Cremona transformation with second degree polynomials

$$x' = \tilde{c}_{10}x + \tilde{c}_{01}y + \tilde{c}_{20}x^2 + \tilde{c}_{11}x\,y + \tilde{c}_{02}y^2$$

$$y' = \bar{c}_{10}x + \bar{c}_{01}y + \bar{c}_{20}x^2 + \bar{c}_{11}x\,y + \bar{c}_{02}y^2$$

Example: Thin sextupole

Consider simple 1D accelerator lattice consisting of linear optics elements (drift spaces, dipoles, and quadrupoles)

$$\mathrm{M}: \quad \begin{bmatrix} x \\ \dot{x} \end{bmatrix}' = \begin{bmatrix} \cos\Phi + \alpha \sin\Phi & \beta \sin\Phi \\ -\gamma \sin\Phi & \cos\Phi - \alpha \sin\Phi \end{bmatrix} \begin{bmatrix} x \\ \dot{x} \end{bmatrix},$$

where $\Phi = \oint \frac{\mathrm{d}s}{\beta(s)} = 2\,\pi\,\nu_0$, followed by a single thin sextupole lens:

$$\mathrm{F}: \quad \begin{bmatrix} x \\ \dot{x} \end{bmatrix}' = \begin{bmatrix} x \\ \dot{x} \end{bmatrix} - \frac{S}{2} \begin{bmatrix} 0 \\ x^2 \end{bmatrix}, \qquad S = \int K_x(s)\,\mathrm{d}s.$$

$$x_0 + \dot{x}_0 + \alpha + \beta + \gamma + \Phi + S - \text{"}[\beta\,\gamma - \alpha^2 = 1]\text{"}$$
$$= 4 \text{ parameters} + 2 \text{ initial conditions}$$

Hénon vs McMillan forms of the map

Hénon form of the map, $F(x) = x^2$

$$x' = x\cos\Phi - [y - F(x)]\sin\Phi$$

$$y' = x\,\sin\Phi + [y - F(x)]\cos\Phi$$

$$\mathrm{T}: \quad \begin{cases} q = x\,\cos\Phi + y\,\sin\Phi \\ p = x, \end{cases}$$

$$\boxed{f(q) = 2\,q\,\cos\Phi + \sin\Phi\,F(q)}\,.$$

McMillan form of the map, $f(q) = a\,q + q^2$

$$q' = p$$

$$p' = -q + f(p)$$

1.2 Symmetric McMillan map

Form of the map

$$Q' = P,$$
$$P' = -Q + F(P),$$
$$F_s(P) = -\frac{B_0\,P^2 + E_0\,P + \Xi_0}{A_0\,P^2 + B_0\,P + \Gamma_0}.$$

Invariant of motion

$$K_s[P,Q] = A_0\,P^2\,Q^2 + B_0\,(P^2\,Q + P\,Q^2)$$
$$+\Gamma_0\,(P^2 + Q^2) + E_0\,P\,Q + \Xi_0\,(P + Q) + K_0$$
$$= \begin{bmatrix} Q^2 \\ Q \\ 1 \end{bmatrix}^{T} \cdot \left(\begin{bmatrix} A_0 & B_0 & \Gamma_0 \\ B_0 & E_0 & \Xi_0 \\ \Gamma_0 & \Xi_0 & K_0 \end{bmatrix} \cdot \begin{bmatrix} P^2 \\ P \\ 1 \end{bmatrix} \right).$$

"Normal" form and intrinsic variables

$$q' = p, \qquad f_0(p) = -\frac{q^2 - a\,q}{\rho\,q^2 + q + 1},$$

$$p' = -q + f(p), \qquad f_\pm(p) = -\frac{r\,q^2 - a\,q}{\pm q^2 + r\,q + 1}.$$

$$\overline{\mathrm{B}} \neq 0: \quad \mathcal{K}_{\mathrm{s}}^{0}[p,q] = \mathcal{K}_0[p,q] + (p^2 q + p\,q^2) + \rho\,p^2 q^2, \quad \rho = \frac{\overline{\Gamma}\,\overline{\mathrm{A}}}{\overline{\mathrm{B}}^2},$$

$$\overline{\mathrm{A}} \neq 0: \quad \mathcal{K}_{\mathrm{s}}^{\pm}[p,q] = \mathcal{K}_0[p,q] + r\,(p^2 q + p\,q^2) \pm p^2 q^2, \quad r = \frac{1}{\sqrt{\rho}},$$

$$\mathcal{K}_0[p,q] = p^2 - a\,p\,q + q^2.$$

2. Perturbation theory

- The one-turn map of 1D accelerator lattice with thin nonlinear lens can be brought to form:

$$q' = p,$$
$$p' = -q + f(p), \qquad f(\epsilon\, p) = a\,\epsilon\, p + b\,\epsilon^2 p^2 + c\,\epsilon^3 p^3 + \ldots.$$

- Looking for an approximate invariant:

$$\mathcal{K}^{(n)} = \mathcal{K}_0 + \epsilon\,\mathcal{K}_1 + \epsilon^2\mathcal{K}_2 + \ldots + \epsilon^n\mathcal{K}_n : \; \mathcal{K}'^{(n)} - \mathcal{K}^{(n)} = \mathcal{O}(\epsilon^{n+1}),$$

where $\mathcal{K}_m$ are homogeneous polynomials of degree $(m+2)$:

$$\mathcal{K}^{(2)} = \mathcal{K}_0[p,q] - \frac{\epsilon\, b}{a+1}\,(p^2\,q + p\,q^2) + \epsilon^2\left[\frac{b^2}{a\,(a+1)} - \frac{c}{a}\right] p^2 q^2.$$

Up to a second order $\mathcal{K}^{(n)}[p, q]$ matches McMillan map

$$\frac{\mathrm{A}}{\epsilon^2} = \frac{b^2}{a\,(a+1)} - \frac{c}{a}, \qquad \frac{\mathrm{B}}{\epsilon} = -\frac{b}{a+1}, \qquad \rho = \frac{\mathrm{A}}{\mathrm{B}^2}.$$

Symmetric McMillan Map:

$$f(q) = -\frac{\mathrm{B}\,q^2 - a\,q}{\mathrm{A}\,q^2 + \mathrm{B}\,q + 1}$$

$$= a\,q + b\,q^2 + c\,q^3 + \frac{b\,(c\,(1+2\,a) - b^2)}{a\,(a+1)}\,q^4 + \mathcal{O}(q^5)$$

Generic thin lens:

$$f(q) = a\,q + b\,q^2 + c\,q^3 + d\,q^4 + \mathcal{O}(q^5)$$

Example: Quadratic Hénon map, $f(q) = a\,q + q^2$

The corresponding second-order approximate invariant is:

$$\mathcal{K}^{(2)}_{\text{SX-2}}[p,q] = \mathcal{K}_0[p,q] - \frac{p^2 q + p\,q^2}{a+1} + \frac{p^2 q^2}{a\,(a+1)},$$

$$f_{\text{SX-2}}(q) = \frac{a\,q^2 + a^2(a+1)\,q}{q^2 - a\,q + a\,(a+1)} = a\,q + q^2 + \mathcal{O}(q^4),$$

with its normal form given by:

$$\mathcal{K}^{(2n)}_{\text{SX-2}}[p,q] = \mathcal{K}_0[p,q] + p^2 q + p\,q^2 + \rho_n\,p^2 q^2,$$

$$\rho_n = \frac{a+1}{a} = \frac{2\,\cos[2\,\pi\,\nu_0] + 1}{2\,\cos[2\,\pi\,\nu_0]}.$$

Atlas of intrinsic parameters

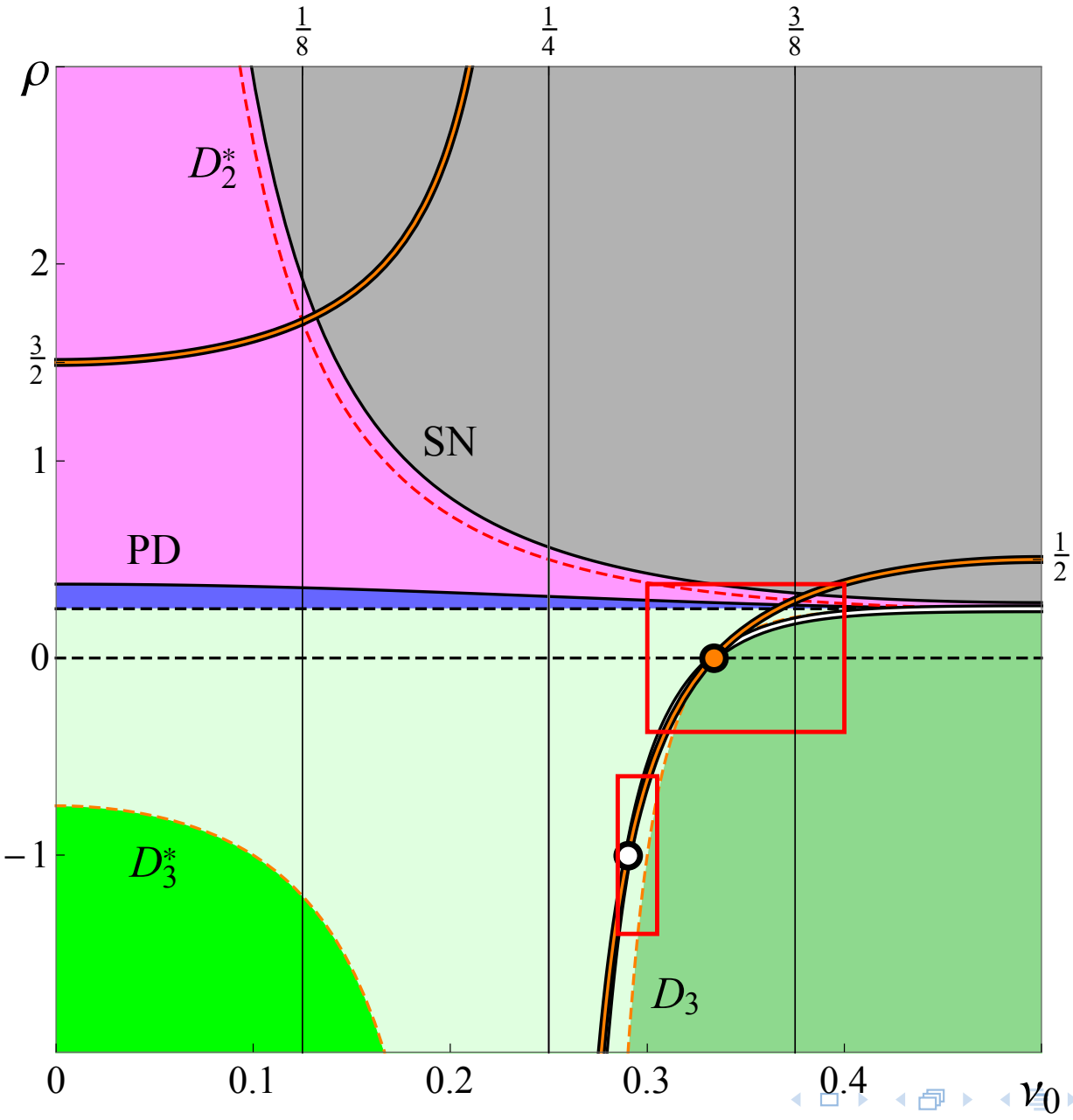

Sextupole and Octupole

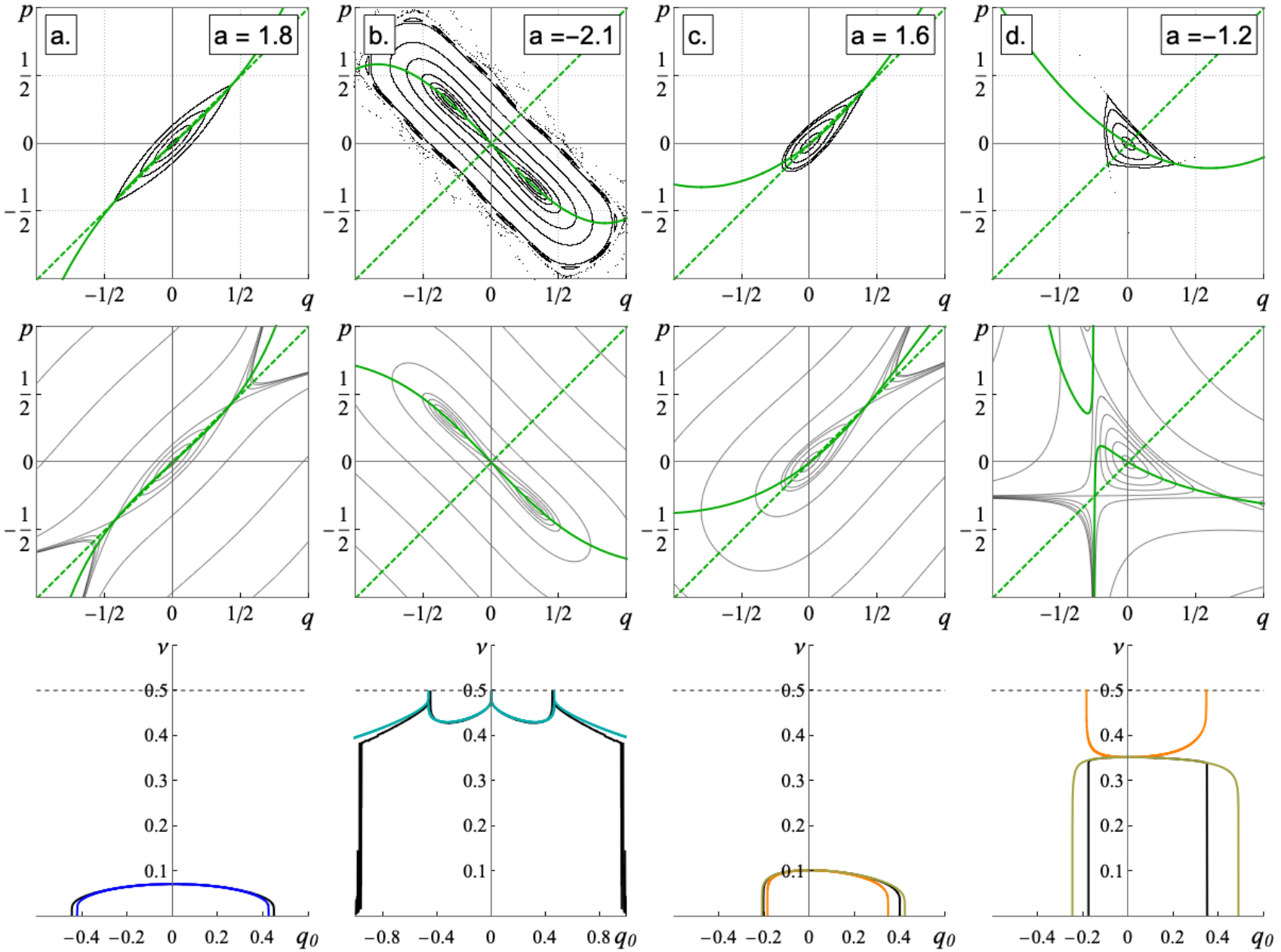

Hénon Stability Diagram

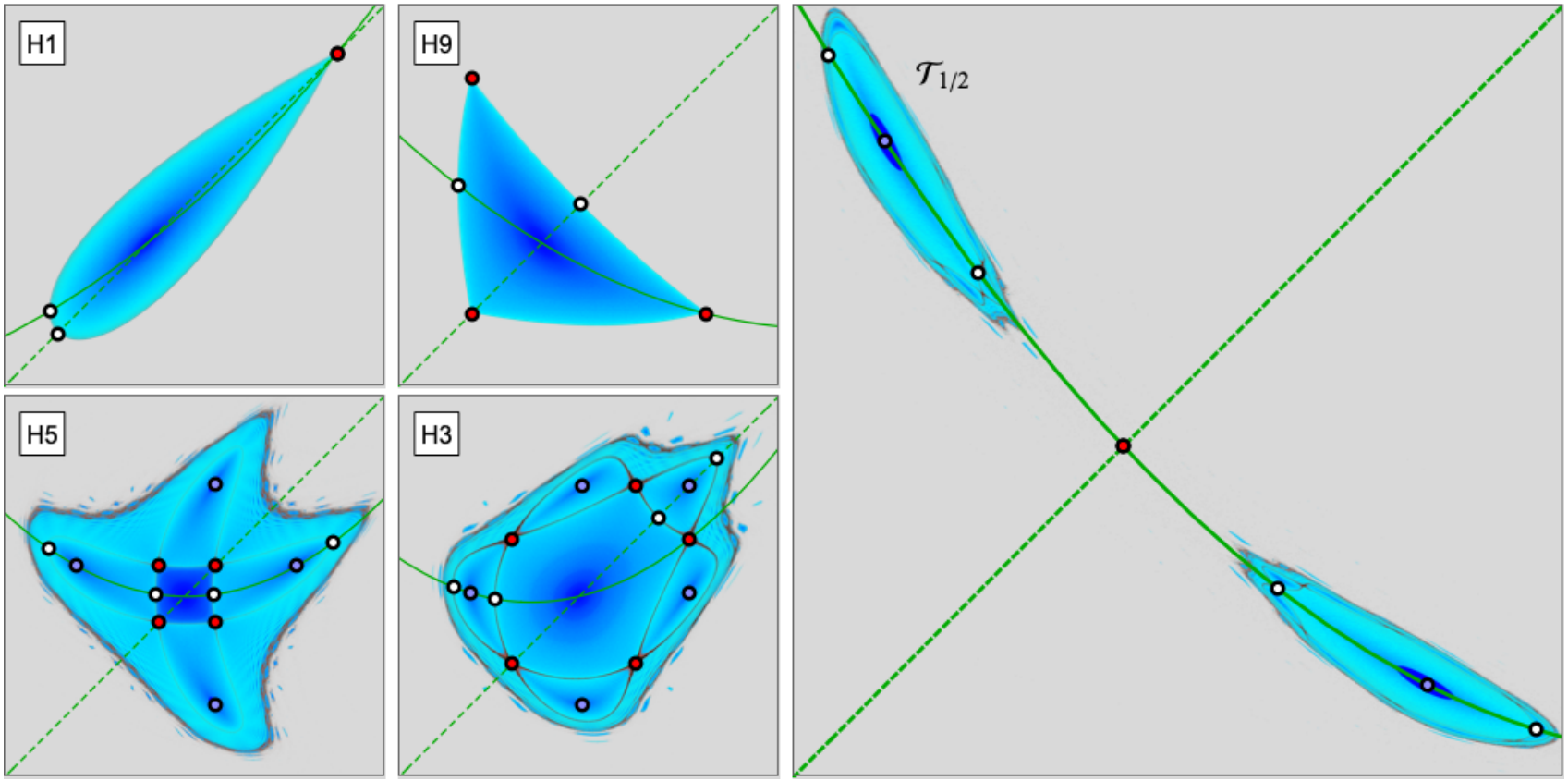

3. Comparison of stability diagrams

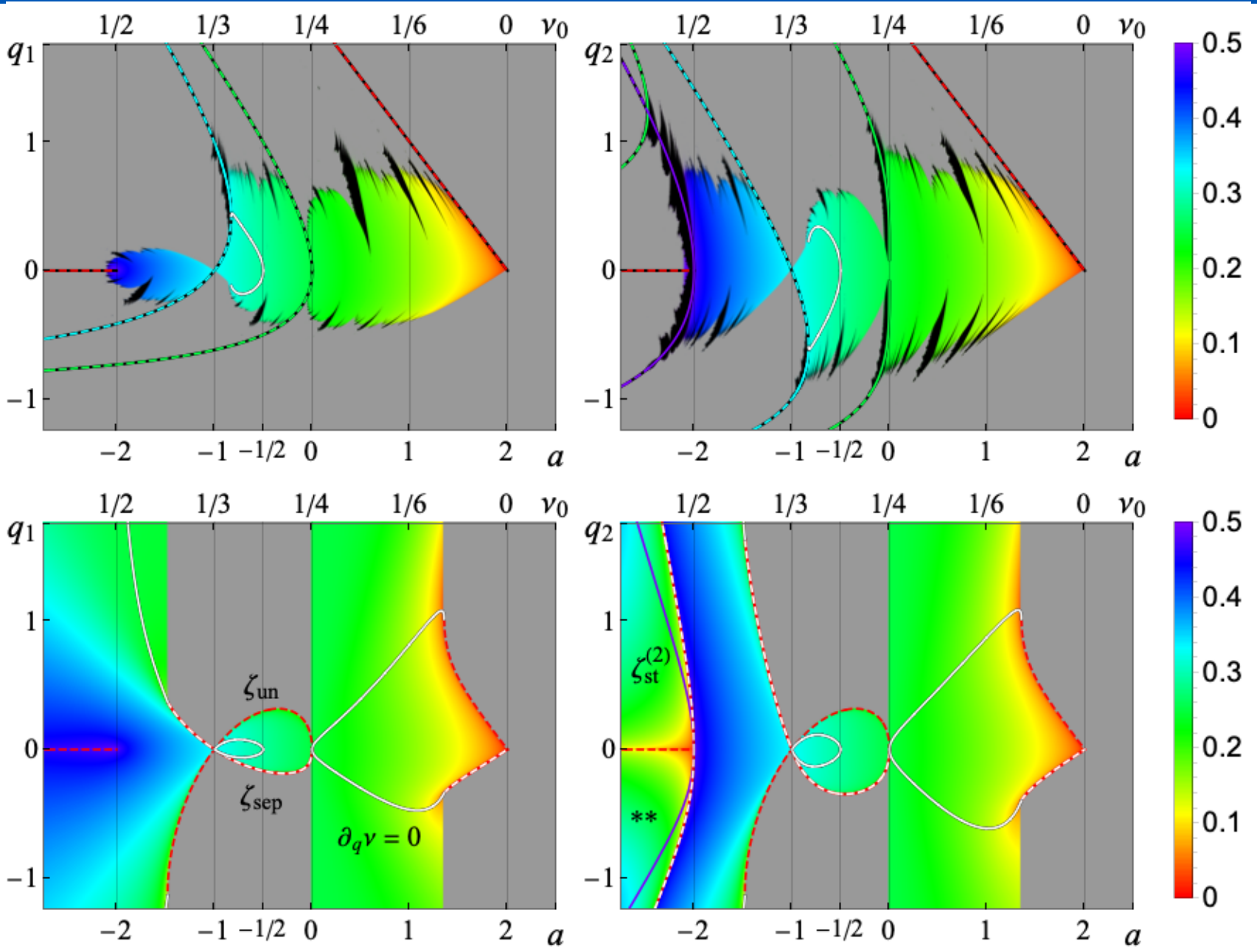

3.1 Integer resonance, $\nu_0 = 0$

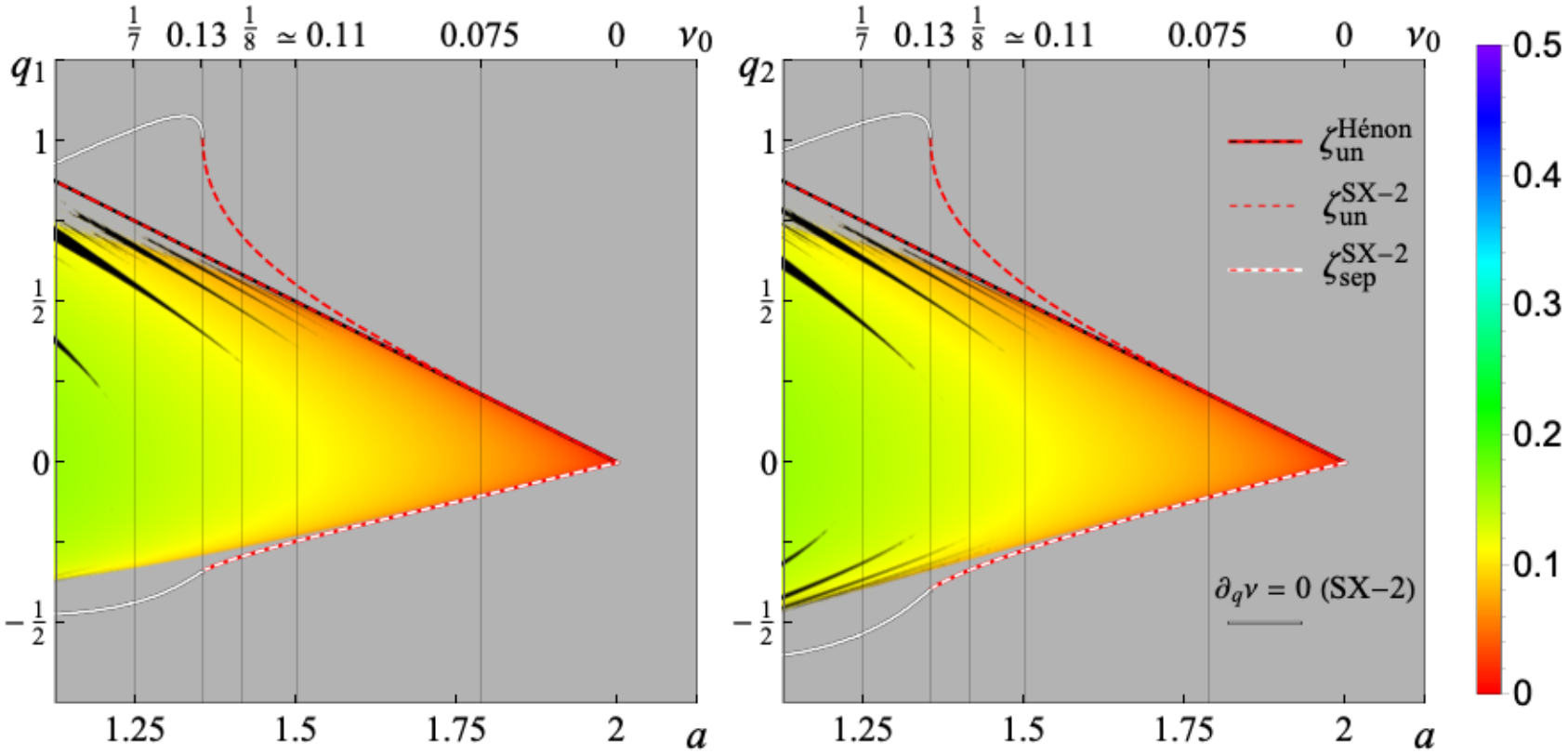

Integer resonance, $\nu_0 = 0$

Comparing fixed points

$$\zeta_{\text{un}}^{\text{Hénon}} = 2 - a, \qquad \zeta_{\text{un}}^{\text{SX-2}} = \frac{3\,a - \sqrt{a\,(8\,a^2 + a - 16)}}{4}$$

we see the accuracy of the model

$$\zeta_{\text{un}}^{\text{Hénon}} - \zeta_{\text{un}}^{\text{SX-2}} = -\tfrac{1}{6}\,\delta r_0^3 + \mathcal{O}(\delta r_0^4), \qquad \delta r_0 = (2 - a).$$

$$\left.\frac{\mathrm{d}\,\zeta_{\text{un}}^{\text{Hénon}}}{\mathrm{d}a}\right|_{\delta r_0 = 0} = \left.\frac{\mathrm{d}\,\zeta_{\text{un}}^{\text{SX-2}}}{\mathrm{d}a}\right|_{\delta r_0 = 0} = -1.$$

However, the SX-2 model also provides a linear estimate for the lower boundary (separatrix location):

$$\left.\frac{\mathrm{d}\,\zeta_{\text{sep}}^{\text{SX-2}}}{\mathrm{d}a}\right|_{\delta r_0 = 0} = \frac{1}{2}.$$

3.2 Half-integer resonance, $\nu_0 = 1/2$

$$\tau\left(\zeta^{(2)}_{\text{Hénon}}\right) = 14 - a\,(a-4), \qquad \tau\left(\zeta^{(2)}_{\text{SX-2}}\right) = \frac{64 + 78\,a + 24\,a^2 + a^3}{a\,(a+1)}.$$

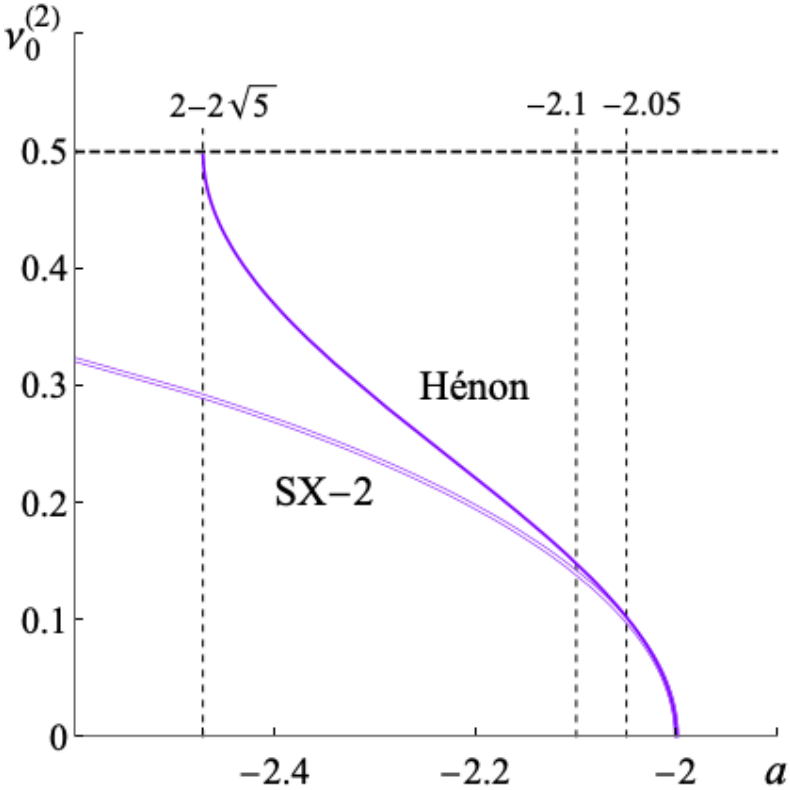

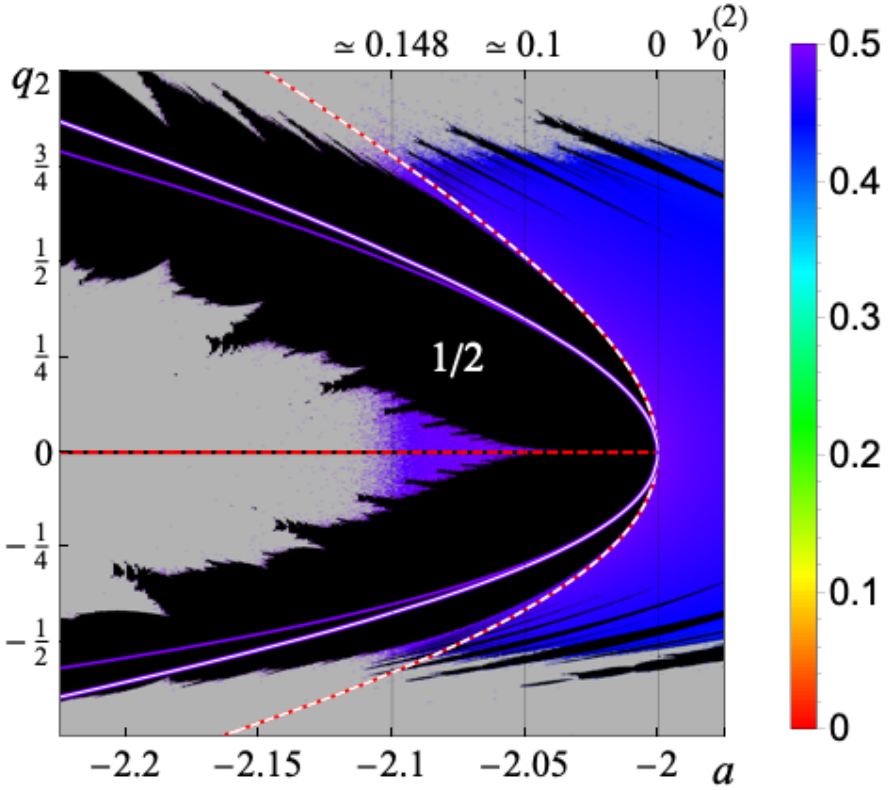

$$\tau\left(\zeta^{(2)}_{\text{Hénon}}\right) - \tau\left(\zeta^{(2)}_{\text{SX-2}}\right) = -4\,\delta r^2_{1/2} + \mathcal{O}(\delta r^3_{1/2}), \qquad \delta r_{1/2} = a + 2.$$

Half-integer resonance, $\nu_0 = 1/2$

Both derivatives tend to infinity at $\delta r_{1/2} = 0$:

$$\left.\frac{\mathrm{d}\,\zeta^{(2)}_{\text{Hénon}}}{\mathrm{d}a}\right|_{\delta r_{1/2}=0} = \left.\frac{\mathrm{d}\,\zeta^{(2)}_{\text{SX-2}}}{\mathrm{d}a}\right|_{\delta r_{1/2}=0} = \infty.$$

Thus, we can invert the dependence $\zeta^{(2)}_{1,2}(a)$ to compare the *terminal* values of parameter a

$$\begin{aligned} a_t^{\text{Hénon}} &= -q - \frac{4}{2+q} &&= -2 - \frac{q^2}{2} + \frac{q^3}{4} - \frac{q^4}{8} + \mathcal{O}(q^5), \\ a_t^{\text{SX-2}} &&&= -2 - \frac{q^2}{2} + \frac{q^3}{4} + \frac{q^4}{8} + \mathcal{O}(q^5). \end{aligned}$$

Observation #1. The region where SX-2 approximation holds aligns with the stability diagram's areas that lack significant mode-locking. In this area, higher-order resonances minimally overlap, and stability is governed by the position of the unstable fixed point.

Observation #2. Similar to the case of integer resonance, we identify two regions of parameter accuracy: "high" and "medium." In the high-accuracy region, where the rotation number for the 2-cycle in the Hénon map is $\nu_0^{(2)} \in (0.1, 0]$, both the unstable fixed point at the origin and $\zeta_{\text{sep}}^{(2)}$ provide good estimates for the mode-locked area. Further from the resonance, where $\nu_0^{(2)} \in (0.148, 0.1]$, $\zeta_{\text{sep}}^{(2)}$ maintains about 15% accuracy, while the fixed point at the origin diverges from the boundary of the mode-locked region. Beyond $\nu_0^{(2)} > 0.148$, most invariant tori associated with orbits around the figure-8 separatrix are destroyed, making the application of perturbation theory at the origin questionable.

3.3 Third-integer resonance, $\nu_0 = 1/3$

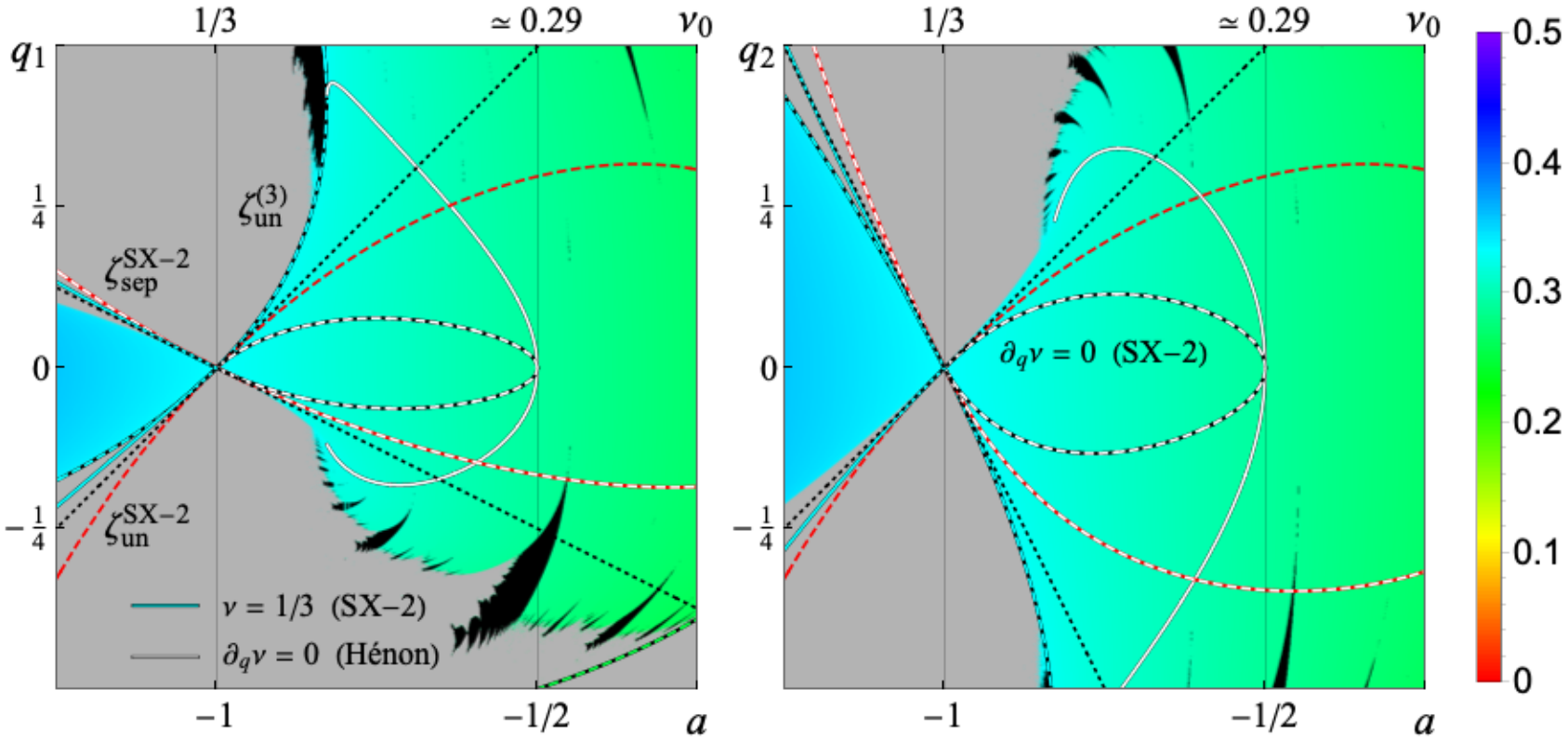

$$\left.\frac{\mathrm{d}\,\zeta_{\rm un}^{\text{SX-2}}}{\mathrm{d}a}\right|_{\delta r_{1/3}=0} = 1, \qquad \left.\frac{\mathrm{d}\,\zeta_{\rm sep}^{\text{SX-2}}}{\mathrm{d}a}\right|_{\delta r_{1/3}=0} = -2^{2s-3}.$$

3.4 Resonance $\nu_0 = 1/4$

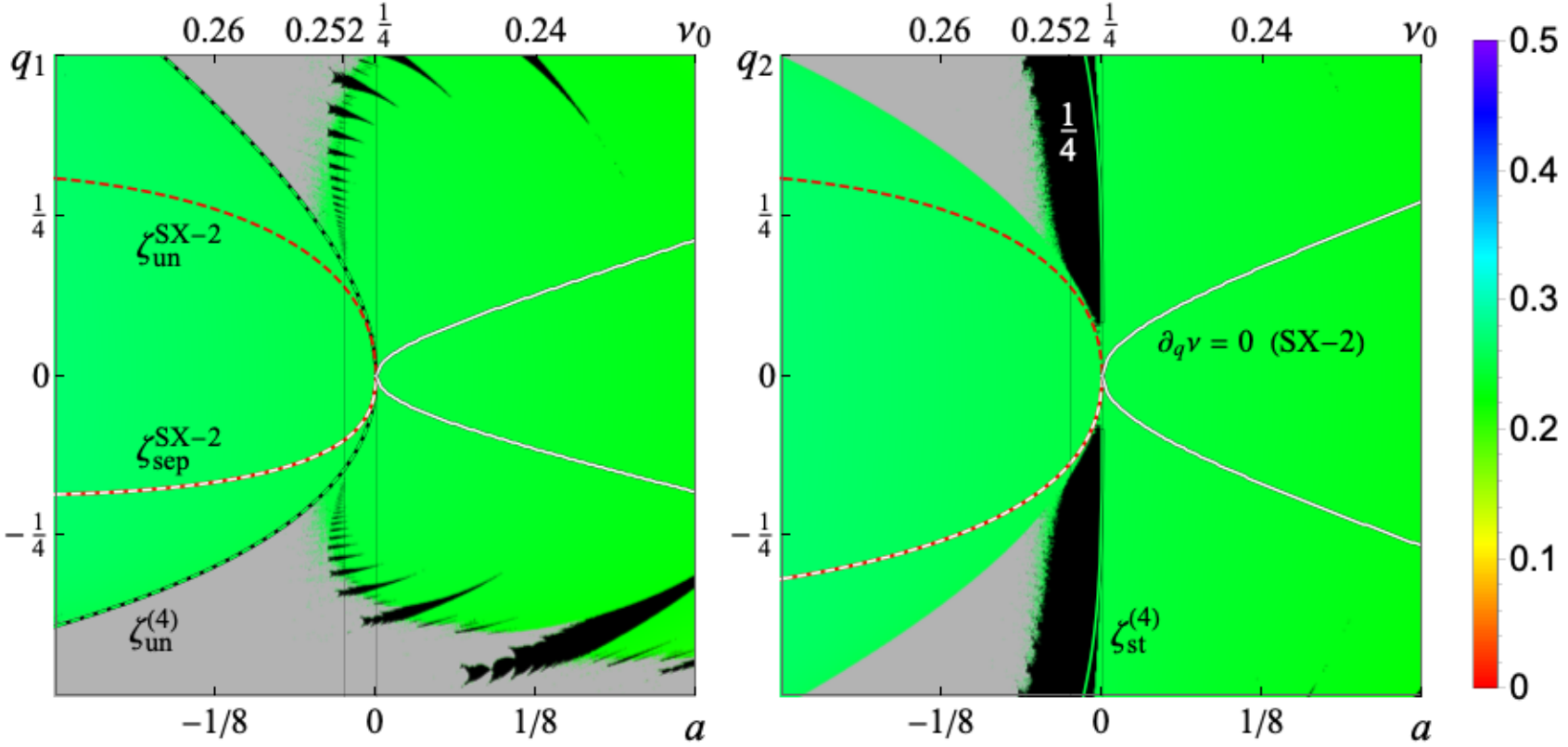

$$a_t^{(4)} = -\frac{q^2}{q+1} = -q^2 + q^3 + \mathcal{O}(q^4) \qquad a_t^{\text{SX-2}} = -q^2 + \mathcal{O}(q^3).$$

$$a_t^{(4)} = -\frac{q^3 + q^2 + 2 - \sqrt{q^4 + 4\,q^3 + 4\,q^2 + 4}}{q\,(q+2)} = -\frac{q^4}{4} + \frac{q^6}{8} + \mathcal{O}(q^7),$$

Observation #3. Interestingly, both mappings exhibit an orbit where $\partial_q \nu = 0$ which appears for $a < -1/2$: solid white for the Hénon map and dashed black/white for the SX-2 model. In the chaotic case, this structure disappears, giving rise to a pair of unstable and stable 3-cycles. In the integrable McMillan SX-2 map, however, it vanishes precisely at the $\nu_0 = 1/3$.

Observation #4. Within the region $\nu_0 \in (0.25, \sim 0.252)$, before the islands separate from the area around the origin, the homoclinic orbit in the SX-2 model provides a fairly accurate estimate along the second symmetry line.

3.5 Mid-range amplitudes: $\nu_0 \neq \frac{1}{5}, \frac{2}{5}, \frac{1}{6}, \frac{1}{7}, \frac{2}{7}, \frac{3}{7}$

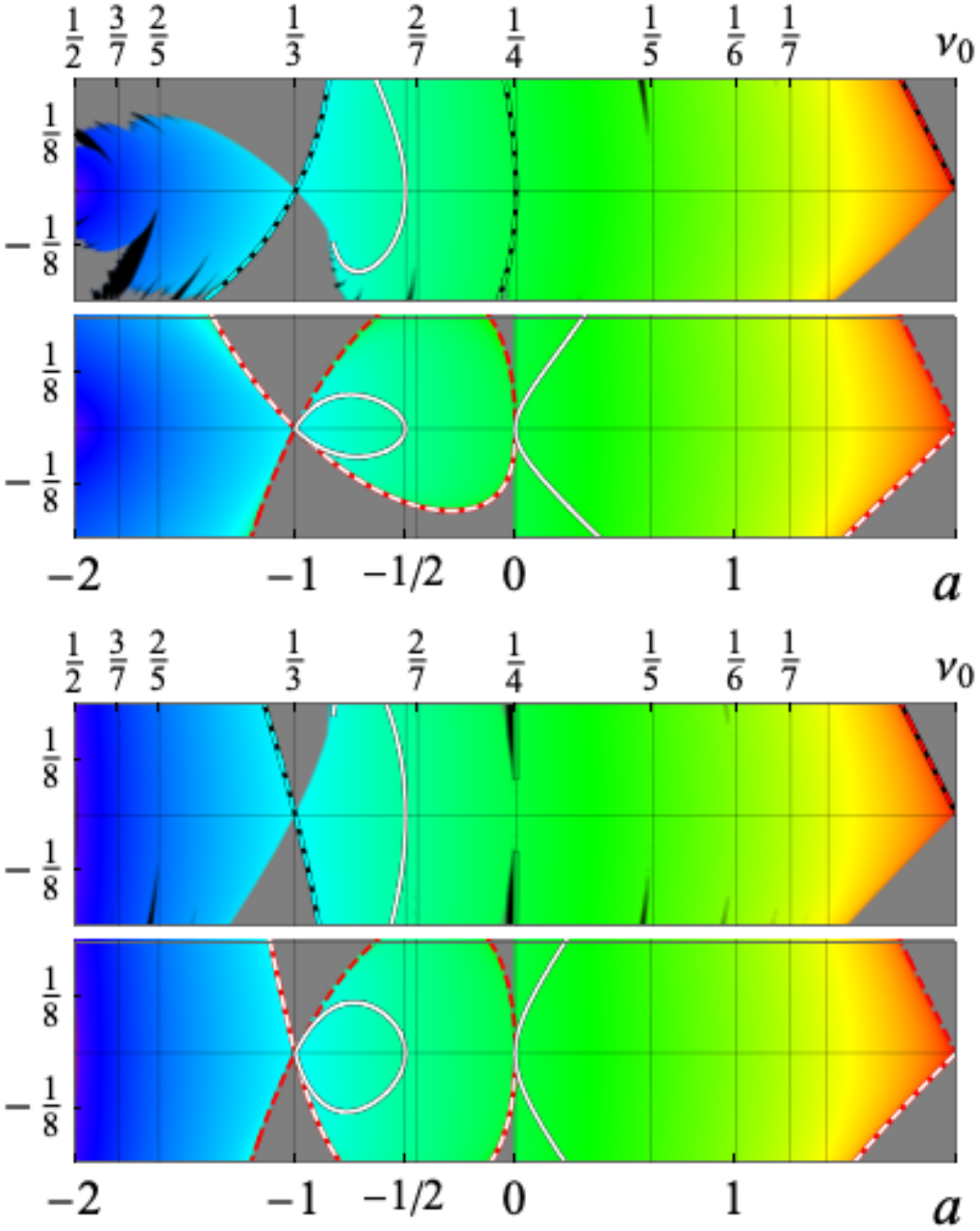

4. Accelerator lattice & thin sextupole (Floquet variables)

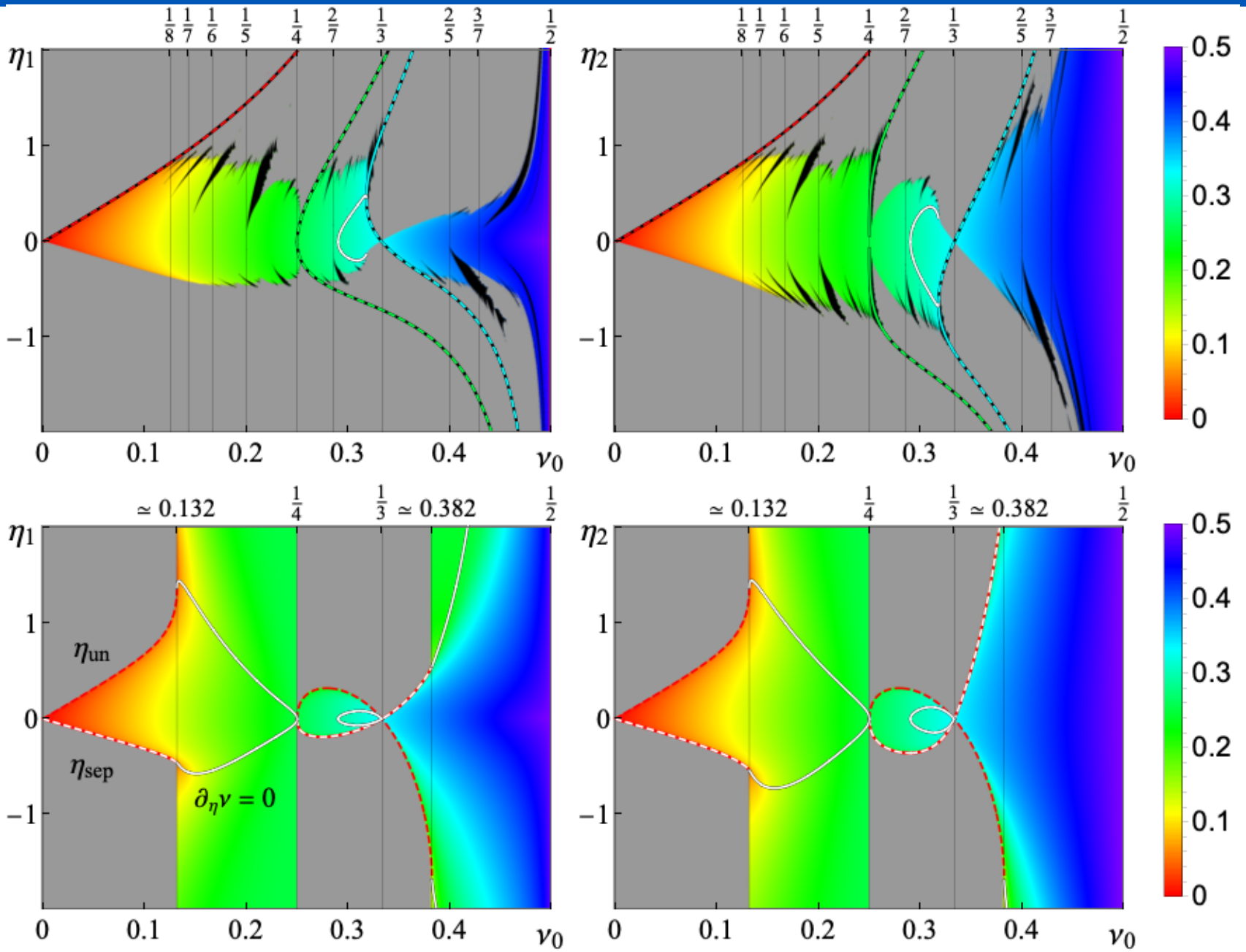

Mid-range amplitudes

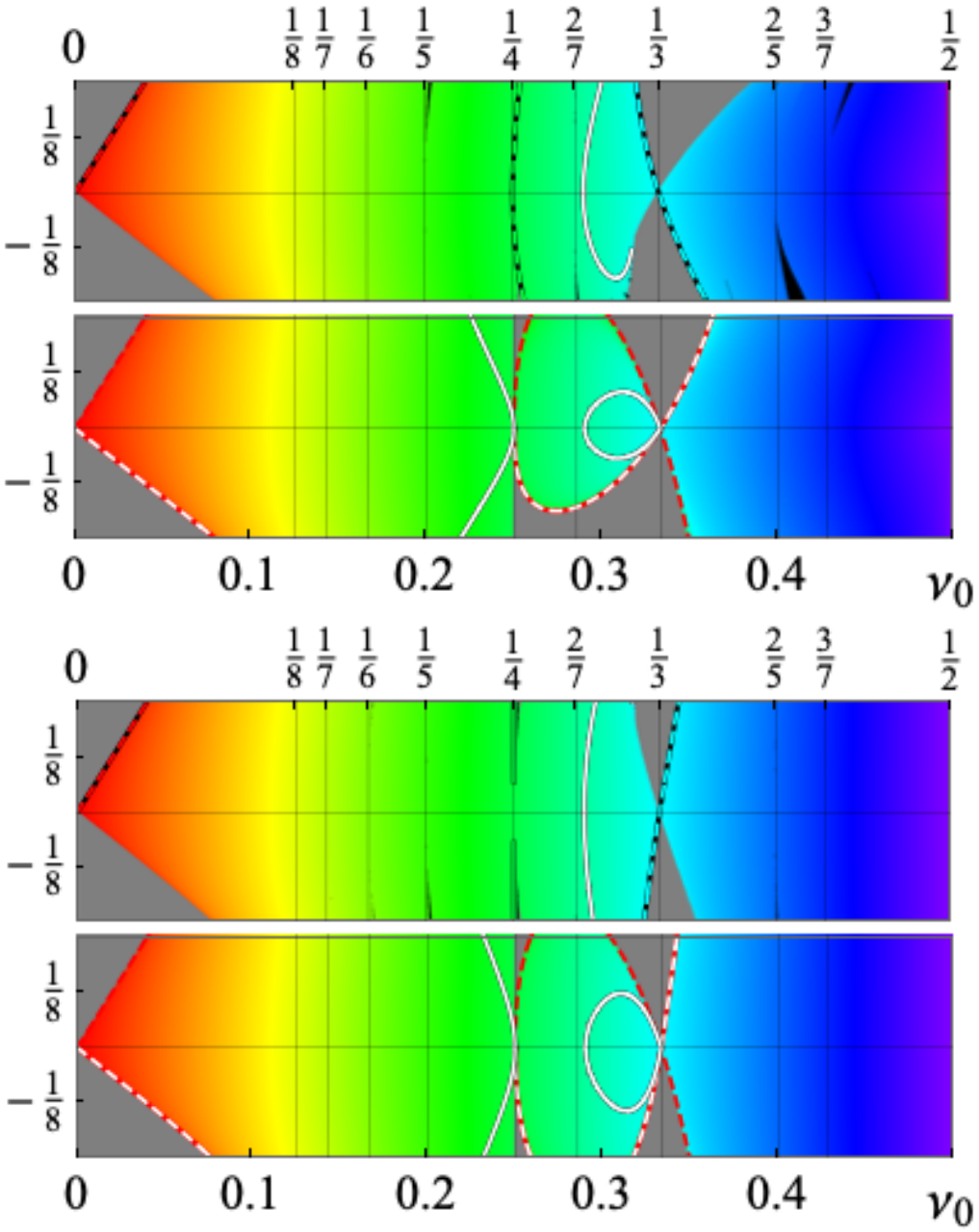

5.1 Summary

This article presents a comprehensive study of the most general symmetric McMillan map, emphasizing its role as a universal model for understanding nonlinear oscillatory systems, particularly symplectic/area-preserving mappings of the plane in standard form with typical force functions. By identifying only two irreducible parameters the linearized rotation number at the fixed point and the coefficient representing the ratio of nonlinear terms in the biquadratic invariant the McMillan map is shown to be both relatively simple and compact, yet highly accurate as an integrable approximation for a broad class of standard-form mappings, especially near main resonances. Through an in-depth analysis of the maps intrinsic parameters, we provide a complete solution to the mapping equations and classify regimes of stable motion. This general model offers analytical expressions for the nonlinear tune shift, rotation number, and action-angle variables, and, also serves as a systematic approach to understanding the qualitative behavior of nonlinear systems under various parameter settings.

5.2 Summary

In the second part of the study, we focus on specific applications of the symmetric McMillan map to model chaotic systems, specifically the quadratic Hénon map and accelerator lattices with thin sextupole magnet. By establishing a connection between these systems, we demonstrate how the McMillan map extends the linear Courant-Snyder formalism, enabling predictions of dynamic aperture and the nonlinear betatron tune (rotation number) as a function of amplitude. We also provide the expression for the approximated single particle emittance of the beam (the phase space area occupied by particles). This work underscores the importance of using integrable systems to accurately model complex nonlinear interactions under certain conditions, reinforcing the relevance of such models in both theoretical research and practical applications.

Thank you for your attention.

Questions?